ACS APPLIED MATERIALS & INTERFACES

RESEARCH ARTICLE

www.acsami.org

Facile Construction of Multicompartment Multienzyme System through Layer-by-Layer Self-Assembly and Biomimetic Mineralization

Jiafu Shi,[†] Lei Zhang,[†] and Zhongyi Jiang[†,‡,*]

[†]Key Laboratory for Green Chemical Technology of Ministry of Education, School of Chemical Engineering and Technology, Tianjin University, Tianjin 300072, P. R. China.

[‡]State Key Laboratory of Bioreactor Engineering, East China University of Science and Technology, Shanghai, China.

Supporting Information

ABSTRACT: In nature, some organelles such as mitochondria and chloroplasts possess multicompartment structure, which render powerful and versatile performance in cascade conversion, selective separation, and energy transfer. In this study, mitochondria-inspired hybrid double membrane microcapsules (HDMMCs) were prepared through synergy between biomimetic mineralization and layer-by-layer (LbL) self-assembly using double templating strategy. The organic inner membrane was acquired via LbL self-assembly of oxidized alginate (o-alginate) and protamine on the $CaCO_3$ template, the silica template layer was then formed onto the inner membrane through biomimetic silicification using protamine as inducer and silicate as precursor, the organic−inorganic hybrid outer membrane was acquired via biomimetic mineralization of titanium precursor. After the $CaCO_3$ template and the silica template are removed subsequently, multicompartment microcapsules with microscale lumen and nanoscale intermembrane space were obtained. The double membrane structure of the HDMMCs was verified by high resolution scanning electron microscopy (HRSEM), and the superior mechanical stability of HDMMCs was demonstrated by osmotic pressure experiment and fluorescence microscopy. A multienzyme system was constructed by following this protocol: the first enzyme was encapsulated in the lumen of the HDMMCs, whereas the second enzyme was encapsulated in the intermembrane space. Compared to encapsulated multienzyme in single-compartment microcapsules (SCMCs) or in free form in aqueous solution, enzymatic activity, selectivity, and recycling stability of HDMMCs-enabled multienzyme system were significantly improved. Because of the inherent gentle and generic feature, the present study can be utilized to create a variety of compartment structures for the potential applications in chemical/biological catalysis and separation, drug/gene delivery systems, and biosensors.

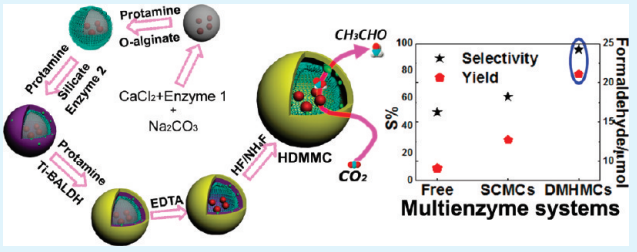

KEYWORDS: hybrid microcapsules, multicompartment structure, layer-by-layer self-assembly, biomimetic mineralization, multienzyme system

1. INTRODUCTION

Compartmentalization is one of the techniques that cells adopt to enable a high level of control over biochemical process. In nature, some cells or organelles possess double membranes with microscale lumen and nanoscale intermembrane space. For instance, mitochondria, the power center of the cell, are of distinct compartment assemblies which include the outer membrane, intermembrane space, inner membrane and lumen. The enzymes for citric acid cycle are confined in the lumen, several other enzymes for cell energy equilibrium (e.g., adenylate kinase) are confined in the intermembrane space. It should be noted that the nanoscale inner membrane was not only utilized for spatial isolation to avoid the negative interference between different enzymes but also for the interfacial enrichment of enzymes and substrates to enhance the reaction velocity, meanwhile, the microscale lumen renders large room for mass and energy storage.[1,2] It could be conjectured that fabricating the multiscale double membrane structure for facile construction of multienzyme system with the inspiration of the elegant structure of mitochondria would be a quite promising research issue.

In recent years, capsules/spheres of double-shelled or multi-shelled structure have spurred increasing interest owing to their unique structures and properties. In general, these capsules/spheres can be categorized into inorganic or organic based on their composition. Inorganic-based capsules/spheres with nanoscale shell-to-shell space are mainly synthesized by hydrothermal or solvothermal method using a hard template (hollow latex,[3] polymer spheres[4] or inorganic silica[5,6]), soft template (surfactant-molecule vesicles[7−9]), an intermediate-templating phase-transformation process,[10,11] and twice-gas-bubble template.[12] The resultant capsules/spheres showed excellent mechanical stability and desired performance in gas sensing,[11,12] water treatment,[7] and Li ion batteries.[8,10] However, the harsh preparation conditions such as high temperature, organic solvents involved in

Received: December 16, 2010
Accepted: February 9, 2011
Published: February 24, 2011

Scheme 1. Construction of Multienzyme System through Synergy of LbL Self-Assembly and Biomimetic Mineralization

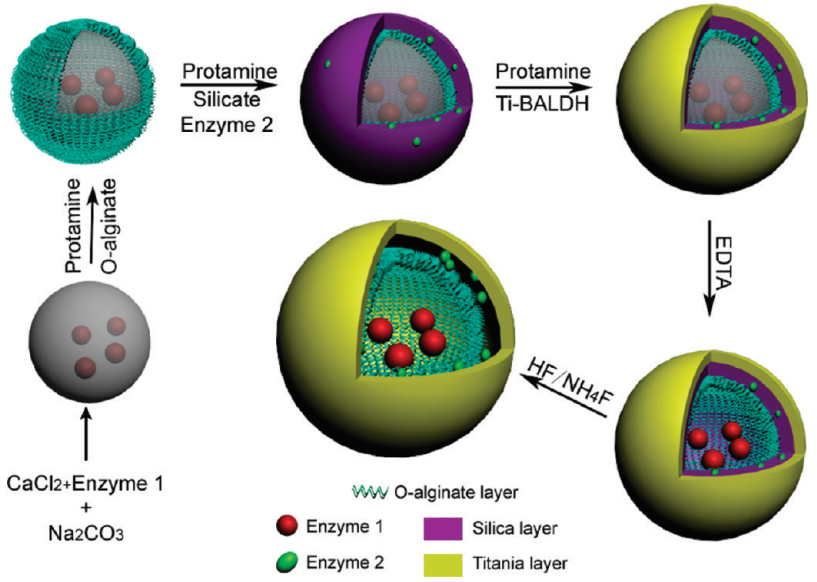

inorganic capsules/spheres preparation greatly hindered its applicability in liable biomacromolecules immobilization and thus multienzyme system construction. In contrast, preparation of organic capsules/spheres of double-shelled or multishelled structure was much less explored. Very recently, tetra and penta-layer polymeric microspheres were prepared by a combined process of sol−gel and distillation-precipitation polymerization, after HF etching of the silica layers.[13,14] Ladet et al. employed a multistep interrupted gelation process under controlled physicochemical conditions to generate complex hydrogels with "onionlike" multimembrane architectures.[15] However, the complexity of the preparation process and harsh conditions for template removal made the above methods difficult or even impossible to encapsulate or entrap the biomacromolecules. By $CaCO_3$-templated layer-by-layer (LbL) self-assembly method, Kreft et al. constructed the multienzyme system by shell-in-shell structured organic microcapsules, where two enzymes were immobilized in two separate compartments and then spatially confined enzymatic reactions were achieved.[16] Because the shell-to-shell space of such-prepared microcapsules is at microscale, it could not serve as an efficient transport hub between the ambient environment and the microcapsule lumen, which dramatically affected the apparent catalytic efficiency of the cascade enzymatic reactions. In addition, the physicochemical properties of the organic capsules/spheres were highly susceptible to environmental fluctuations (e.g., pH value, temperature, or shear stress), causing the instability of physical structure and operation performance. It could be assumed that if organic capsules/spheres are utilized for the multienzyme system construction, the enzyme leakage will become a serious issue. Incorporating inorganic moiety into the matrix of organic capsules/spheres seems a feasible and promising solution.

In the past decade, biomineralization/biomimetic mineralization, as a novel, mild and green platform technology for hybrid materials synthesis,[17,18] has been successfully utilized to prepare robust and bioactive organic−inorganic hybrid microcapsules.[19−23] For example, to enhance the cell viability, Choi et al have conducted silica encapsulation of individual yeast cells by alternate LbL deposition of polycations and polyanions onto the surface of yeast and the subsequent biomimetic silicification.[19] In recent years, our group has dedicated to prepare a variety of mechanical stable hybrid microcapsules using biomimetic and bioinspired approaches.[20,21,23] It was found that protamine could induce the formation of silica and titania nanoparticles from water-soluble precursors in a facile way.[24,25] On the basis of this finding, spatially separated multienzyme cascade system and efficient cascade enzymatic reaction were realized. For instance, polymersome nanocapsules have been utilized for positional location of multienzyme in its lumen (glucose oxidase, GOx), in the membrane (candida antarctica lipase B, CalB) and on the surface (horseradish peroxidase, HRP), respectively.[26] DNA scaffold has been utilized to immobilize GOx/HRP for efficient enzymatic conversion.[27] Polyelectrolyte shell-in-shell microcapsules has been served a novel tool for integrated, spatially confined multienzymatic reactions.[16] Capsules-in-bead scaffold has been fabricated in our previous work for establishing multienzyme system.[28] However, as far as we are concerned, biomimetic mineralization has not yet been utilized for the preparation of capsules with double membrane structure (hereafter, the word "membrane" was borrowed to infer that the inner and outer shell of the hybrid double membrane microcapsules (HDMMCs) possess selective permeability to small molecules[29,30]), and for the construction of multienzyme systems.

In this study, we have prepared the robust multicompartment HDMMCs and constructed an efficient multienzyme system through the synergy of LbL self-assembly and biomimetic mineralization (as shown in Scheme 1). In detail, oxidized alginate (o-alginate) layer is formed through LbL self-assembly on the protamine-soaked enzyme (the first enzyme)-containing $CaCO_3$ microspheres. The assembly process can be repeated several times for the specific requirement. Then, protamine layer is formed on the o-alginate surface through dip-coating, inducing the hydrolysis and condensation of silicate precursor to form silica layer. Another kind of enzyme (the second enzyme) in the silicate aqueous solution is entrapped within the silica layer. Next, protamine is adsorbed on the surface of the silica layer to induce the formation of titania layer from water-soluble titanium precursor. Finally, the $CaCO_3$ template and the silica template are

sequentially removed by EDTA and HF/NH_4F, and the HDMMCs with protamine/o-alginate multilayers as the inner membrane and protamine/titania layer as the outer membrane are acquired. The structure in particular the thickness of the inner membrane and outer membrane, intermembrane space, and the enzymes loading capacity can be conveniently tuned. As demonstration, a multienzyme system containing formate dehydrogenase (FateDH, enzyme 1) and formaldehyde dehydrogenase (FaldDH, enzyme 2) was explored to for converting carbon dioxide (CO_2) into formaldehyde.

2. MATERIALS AND METHODS

2.1. Materials. Protamine sulfate from salmon, poly(sodium 4-styrenesulfonate) (PSS, MW ca. 70 000), Ti (IV) bis-(ammonium lactate) dihydroxide (Ti-BALDH, 50 wt % aqueous solution), fluorescein isothiocyanate (FITC), rhodamine B, formate dehydrogenase from from *Candida boidinii* (FateDH, EC.1.2.1.43, 3.33 U mg^{-1}), formaldehyde dehydrogenase from *Pseudomonas putida* (FaldDH, EC.1.2.1.46, 11.0 U mg^{-1}), and reduced nicotinamide adenine dinucleotide (NADH, 98%) were purchased from Sigma-Aldrich Chemical Co.. Sodium silicate (Na_2SiO_3), tris(hydroxymethyl)amiomethane (Tris), hydrochloric acid(HCl), ethylenediaminetetraacetic acid (EDTA), hydrofluoric acid (HF aqueous solution, 40 w/v%), ammonium fluoride (NH_4F) and sodium chloride (NaCl) were obtained from Guangfu Reagent Chemicals Co. Ltd. (Tianjin, China). Sodium alginate was obtained from Jiangtian Reagent Chemicals Co. Ltd. (Tianjin, China). Preparation of o-alginate was briefly described in the Supporting Information. All other reagents were analytical grade and used without further purification.

2.2. Construction of Multicompartment Multienzyme Hybrid System. The multicompartment multienzyme hybrid system was constructed via biomimetic mineralization and LbL self-assembly. At the beginning, enzyme (FateDH)-containing $CaCO_3$ microspheres were used as sacrificial templates, which were prepared according to the coprecipitation method described previously in the literature.[31] Briefly, PSS (4.5 mg) and enzyme (1.0 mg) were completely dissolved in $CaCl_2$ solution (1.5 mL, 0.33 M) in a beaker at room temperature. Then, an equal volume of Na_2CO_3 solution (0.33 M) was instantly added into the beaker under magnetic agitation and stirred continuously for 30s. After settled without stirring for 25−30 min, the deposit was centrifuged, and washed twice with deionized water. Finally, enzyme-containing $CaCO_3$ microspheres with spherical shape about 4 μm in size were obtained. Next, these $CaCO_3$ microspheres were homogeneously dispersed in 2 mL of protamine aqueous solution (3 mg mL^{-1}, pH 6.0−7.0). After shaking for 15 min, $CaCO_3$ microspheres coated with protamine were collected by centrifugation, and rinsed twice with water to remove the residual protamine. Subsequently, these microspheres were suspended in 2 mL NaCl-containing o-alginate solution (3 mg mL^{-1}, pH 6.0−6.5), and shaken for 15 min. After centrifuging and washing, $CaCO_3$ microspheres coated with one protamine layer and one o-alginate layer were obtained. This procedure was repeated to deposit 2 bilayers of protamine/o-alginate. The obtained microspheres were then soaked in protamine solution, followed by soaked in enzyme (FaldDH)-containing silicate solution (2 mL, pH 7.0−8.0) to obtain the silica layer as the second template. The formation of the titania outer membrane layer was similar to that of silica layer, where the Ti-BALDH (2 mL, 50 mM, pH 7.0) aqueous solution replaced silicate aqueous solution.

Finally, multicompartment hybrid multienzyme system was acquired after $CaCO_3$ and silica templates were removed. More detailedly, the microscale lumen was formed via the removal of $CaCO_3$ template through incubating microspheres in EDTA solution (0.02 M, pH 7.0, 4 °C, 15 min), and the nanoscale intermmebrane space was formed via the removal of silica template through incubating $CaCO_3$-removed microcapsules in HF/NH_4F solution (ca. 0.5 M/2 M, pH5.5, 4 °C, 3 min). Then, the obtained HDMMCs were washed with deionized water for several times. Additionally, for comparison purpose, $(protamine/o\text{-}alginate)_4$ SCMCs were fabricated via alternative adsorption of protamine and o-alginate for 8 times on the $CaCO_3$ microspheres to encapsulate two kinds of dehydrogenases. The $CaCO_3$ microspheres were then removed through incubating in EDTA solution (0.02 M, pH 7.0, 4 °C, 15 min)

2.3. Enzymatic Conversion of CO_2 to Formaldehyde. Conversion of CO_2 to formaldehyde was conducted in aqueous solution with free or immobilized enzymes. The pressure was maintained at 0.3 MPa. The formaldehyde concentration was determined by gas chromatography (GC) equipped with a flame ionization detector (FID; Hewlett-Packard, model HP-6890). All the measurements were repeated three times. It should be mentioned that the formic acid concentration was too low to be detected. Conversion of CO_2 by HDMMCs was performed according to the following procedure. Briefly, HDMMCs−containing solution (0.5 mL) was bubbled with CO_2 for 0.5 h before adding 0.5 mL NADH solution to initiate the enzymatic reaction (the actual amount of encapsulated FateDH and FaldDH was both 0.3 mg, with a final NADH concentration of 50−200 mM). For comparison, the same amount of free enzymes and enzymes encapsulated in SCMCs had also undergone the catalytic activity evaluation. The formaldehyde product (the enzyme units added to each multienzyme system were equal, μmol), reaction rate (NADH consumption rate of the cascade reaction, ν, μmol $(min)^{-1}$ $(mg(enzyme))^{-1}$) and selectivity (S, %) was calculated based on eq 1, 2 and 3:

$$\text{formaldehyde product } (\mu\text{mol}) = V_{\text{system}} C_{\text{formaldehyde}} \quad (1)$$

$$\nu_t \ (\mu\text{mol min}^{-1} \ (\text{mg of enzyme})^{-1}) = \frac{V_{\text{system}}(C_{\text{NADH},t} - C_{\text{NADH,t}-\Delta t})}{M_{\text{enzyme}}\Delta t}100 \quad (2)$$

$$S(\%) = \frac{2C_{\text{formaldehyde}}}{\Delta C_{\text{NADH}}}100 \quad (3)$$

Where V_{system} was the solution volume of the system (L), $C_{\text{formaldehyde}}$ was the concentration of formaldehyde after the enzymatic reaction (M), ν_t was the reaction rate at time t (μmol min^{-1} (mg of enzyme)$^{-1}$), $C_{\text{NADH},t-\Delta t}$ was the NADH concentration at the time of $t - \Delta t$ (M), $C_{\text{NADH},t}$ was the NADH concentration at the time of t (M), and ΔC_{NADH} was the NADH consumed during the whole enzymatic reaction (M), which was determined by the NADH concentration before and after reaction at 340 nm using a UV spectrophotometer.

2.4. Characterizations. FTIR spectra of the microcapsules were obtained on a Nicolet-6700 spectrometer. 32 scans were accumulated with a resolution of 4 cm^{-1} for each spectrum. The surface zeta-potentials of PSS-doped $CaCO_3$ microspheres and the inner membrane with different bilayers were measured in water using a Brookhaven zeta-potential analyzer. Five parallel measurements were conducted for each sample, and the average value was adopted. HRSEM images were recorded using a field emission scanning electron microscope (FESEM, Nanosem 430). Elemental analysis was accomplished by energy dispersive spectroscope (EDS) attached to FESEM. TEM observation was performed on a JEM-100CX II instrument (bar: 1 μm). Fluorescence microscope images were taken using an Olympus BX51 microscope with a 100 × oil immersion objective lens (Olympus, Tokyo, Japan). The pore-size distribution of the microcapsules was determined by nitrogen adsorption−desorption isotherm measurements performed at 77 K on a Tristar 3000 gas adsorption analyzer. Pore-size distribution curves were calculated on the basis of the adsorption branch of nitrogen isotherms using the Barrett−Joyner−Halenda (BJH) method.

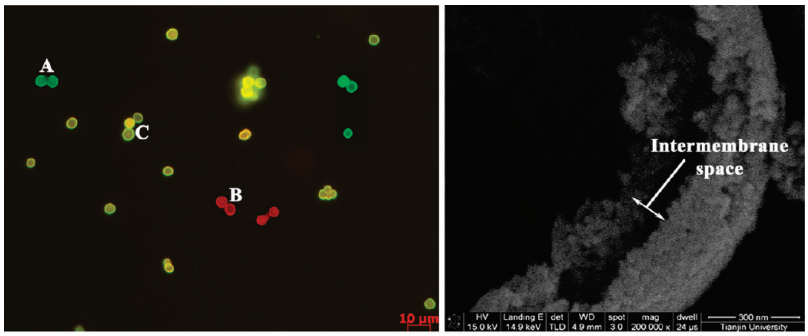

Figure 1. (a) Fluorescence microscope images of HDMMCs with (A) only FITC-labeled inner membrane, (B) only rhodamine B-labeled outer membrane, and (C) FITC-labeled inner membrane and rhodamine B-labeled outer membrane; (b) HRSEM image of the HDMMC.

Enzyme loading capacity of the intermembrane space was determined by using BSA as model protein instead of enzyme due to the similar pI value (ca. 5.0). More detailedly, the loading capacity (LC_{BSA}, $\mu g\ mg^{-1}$) was calculated according to the eq 4

$$LC_{BSA} = \frac{M_{BSA,\ immobilize\ d}}{M_{HDMMCs}} \quad (4)$$

Where $M_{BSA,\ immobilized}$ was the mass of immobilized BSA, (μg), and M_{HDMMCs} was the mass of HDMMCs, (mg). $M_{BSA,\ immobilized}$ was calculated by measuring the concentration of BSA in the supernatant before and after immobilization (20 ± 2 °C). To test the permeability of HDMMCs, we added BSA-containing inner membrane (BSA in the lumen) and HDMMCs (BSA in the intermembrane space) into 1 mL Tris−HCl (0.05 M, pH 7.0), and incubated them at room temperature for a period of time followed by centrifugation. The content of BSA in the supernatant was then determined by the micro-Bradford method using a UV spectrophotometer (Hitachi U-2800) as the detector.

3. RESULTS AND DISCUSSION

3.1. Preparation and Characterization of HDMMCs. Fluorescence images with three types of fluorescent dye-labeled HDMMCs were acquired to probe the successful preparation of the HDMMCs. FITC-labeled protamine was chosen for the fabrication of the inner membrane (FITC-labeled inner membrane) and rhodamine B-labeled protamine was chosen for the fabrication of the outer membrane (rhodamine B-labeled outer membrane). For comparison, HDMMCs with only FITC-labeled inner membrane or only rhodamine B-labeled outer membrane were also fabricated. Next, these three types of the HDMMCs were mixed and observed through fluorescence microscopy: HDMMCs with only FITC-labeled inner membrane emitted green fluorescent signal (Figure 1aA), the HDMMCs with only rhodamine B-labeled outer membrane emitted red fluorescence signal (Figure 1aB), whereas two-fluorescent dye-labeled HDMMCs emitted yellow fluorescent signal, a combination of red and green fluorescent signals (Figure 1aC).[32] Figure 1aC and 1b (cross-section of the HDMMC) clearly displayed the double membrane structure and nanoscale intermembrane space of the microcapsules.

The formation mechanism of the inner membrane was tentatively analyzed by using FTIR and zeta zeta-potential spectra. As shown in Figure 2a (the inner membrane curve), the typical absorbance of COO^- groups at 1410 cm^{-1} and amino groups at 1650 cm^{-1} confirmed the presence of o-alginate and protamine.[23] The absence of aldehyde groups at 1720 cm^{-1} in the inner membrane revealed the depletion of aldehyde groups on o-alginate through the Schiff's base reaction with amino groups on protamine. In Figure 2b, an alternative negative and positive zeta potential of the inner membrane as a function of layer number ranging from −20 mV to 20 mV revealed the interlay electrostatic interaction. Therefore, both the electrostatic and covalent interactions were involved in the inner membrane fabrication. Figure 2c manifested that the inner membrane possessed hollow nature and intact structure after $CaCO_3$ removal. The polygonal shape and folds are characteristics of the organic inner membrane, resulting from the water loss in polymer network. More importantly, energy dispersive spectroscopy (EDS) analysis indicated the presence of C, O, and S elements and absence of Ca element, which confirmed that the $CaCO_3$ template was removed completely. Additionally, HRSEM image (Figure 2d) indicated that the inner membrane possessed a dense surface with a membrane thickness of less than 100 nm.

The thickness of the intermembrane space could be tuned by the concentration of silicate as shown in Figure 3. In a typical experiment, different concentrations (10, 30, 50, and 70 mM) of silicate were employed to prepare the silica template layer by biomimetic silicification process. The thickness of the intermembrane space was detected by measuring the thickness of the silica layer through HRSEM images. From Figure 3, the thickness increased from 70 to 140 nm with the increase in the silicate concentration from 10 to 70 mM, which is in good agreement with the previous observation from Livage's group.[33,34] Considering the aggregation behavior of silica particles, a silicate concentration of 50 mM was selected for intermembrane space construction.

The elemental and morphological analysis of the outer membrane was shown in Figure 4a. Compared with the inner membrane in Figure 2c, the outer membrane possessed a diameter of ca. 4 μm with an intact, regular spherical shape, and exhibited higher mechanical stability during water evaporation. Moreover, energy dispersive spectroscopy (EDS) of the outer membrane clearly revealed the presence of Ti element and absence of Si element, indicating the actual deposition of titania[35] and complete removal of silica template. Compared with the inner membrane in Figure 2d, the outer membrane was much thicker (ca. 200 nm seen from Figure 4b) and possessed asymmetrical inner surface and outer surface (Figure 4c,d).

For enzyme compartmental encapsulation purpose, the HDMMCs must serve two critical functions: (1) both the inner

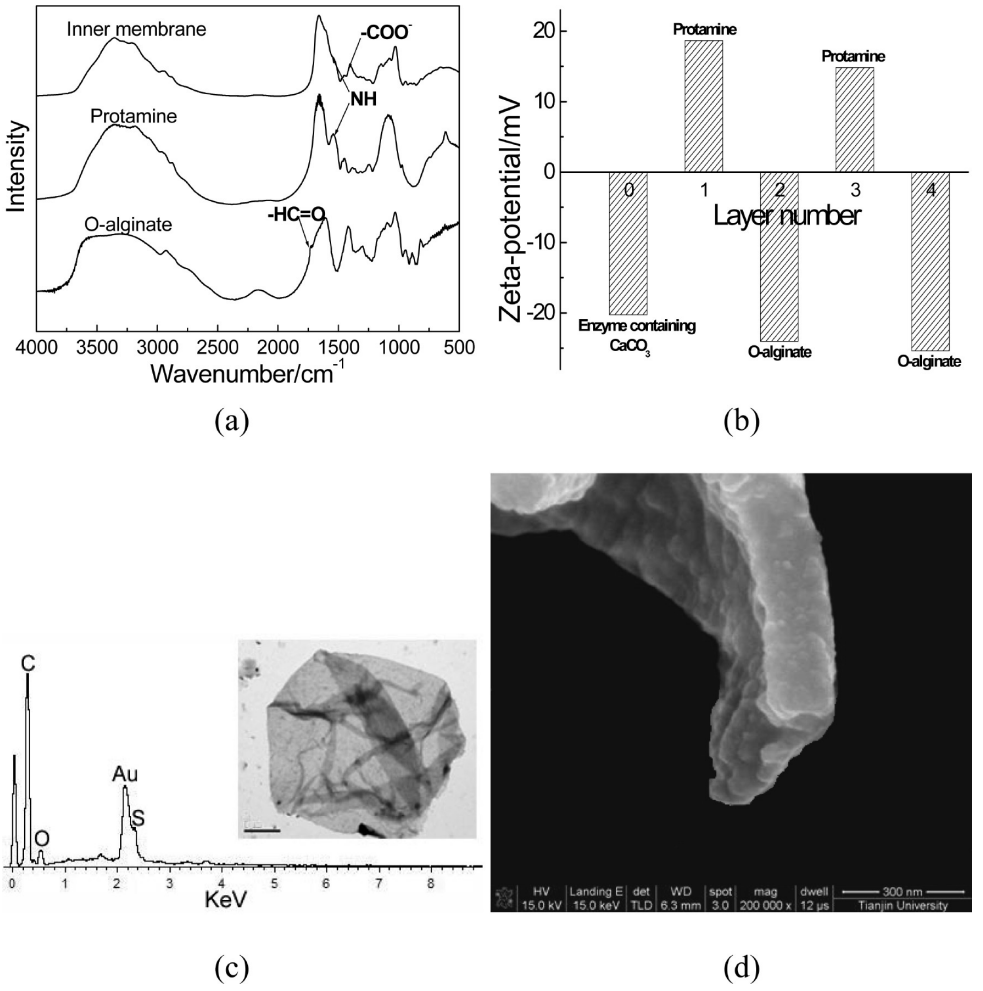

Figure 2. Characterization of the inner membrane: (a) FTIR spectra of o-alginate, protamine, and inner membrane (without PSS during preparation); (b) surface zeta-potential of the inner membrane as a function of layer number; (c) TEM images (bar: 1 μm) and EDS spectra of the inner membrane; and (d) HRSEM image of the inner membrane.

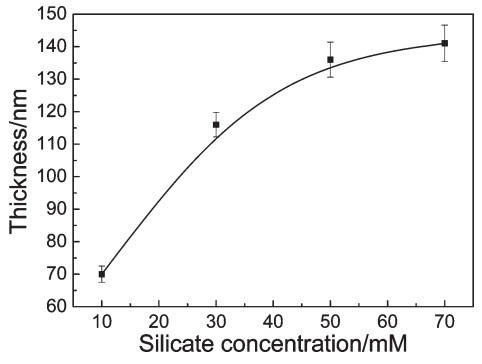

Figure 3. Thickness of the intermembrane space as a function of silicate concentration.

membrane and outer membrane should totally prevent enzymes from leaking; (2) substrates and products can freely diffuse inside and outside the HDMMCs. Thus, BET analysis was employed to determine the surface area, pore volume, and pore size distribution of the inner membrane and HDMMCs. The nitrogen adsorption isotherms of the inner membrane (Figure 5a) and HDMMCs (Figure 5b) both showed type IV characteristics with type H3 hysteresis loop, which indicated the presence of a highly interconnected and slit-shaped pores within the microcapsules.[36] The specific surface area and pore volume of the inner membrane were 56.07 m^2/g and 0.25 cm^3/g, respectively. Meanwhile, the surface area and pore volume of the HDMMCs were 53.02 m^2/g and 0.29 cm^3/g, respectively. The BJH pore size distribution with primary peaks at 2.2 and 30 nm was attributed to the porosity of the outer and inner surfaces of the outer membrane. These results meant that the semipermeability of the HDMMCs could allow substrates (and products) molecules (hydrodynamic diameter were all less than 1 nm) to enter and leave the lumen and intermembrane space rapidly, whereas enzyme molecules (hydrodynamic diameter were ca. 7−10 nm) were substantially retained (the relevant experiment data were shown in Figure S3 in the Supporting Information).

High mechanical stability to resist shear stress and osmotic pressure was another important property of the HDMMCs. Four types of microcapsules were prepared for the mechanical stability testing: $(Protamine/PSS)_4$ SCMCs, $(Protamine/O\text{-}alginate)_4$ SCMCs, organic DMMCs with double $(Protamine/O\text{-}alginate)_2$ membranes, and HDMMCs with $(Protamine/O\text{-}alginate)_2$ inner membrane and (Protamine/Titania) outer membrane. The shape of the microcapsules gradually changed as the osmotic pressure outside the microcapsules increased. Starting with

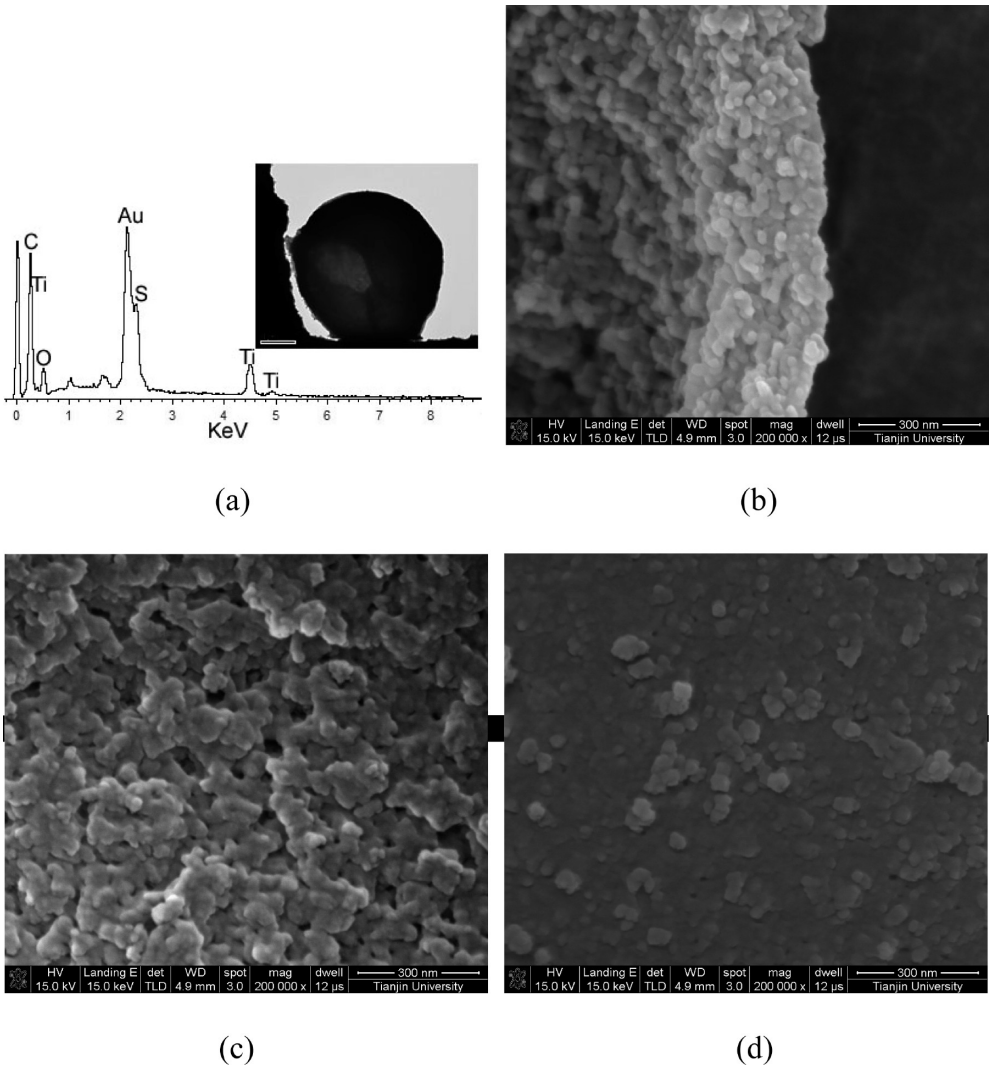

Figure 4. (a) TEM image (bar: 1 μm) and EDS spectrum of the HDMMC; (b) HRSEM images of the outer membrane, (c) inner surface and (d) outer surface of the outer membrane.

perfect spherical structure, a stepwise increase in concentration (4, 8, 12, and 20 wt %) of PSS led to permeation of water from the inside to the outside and concomitant deformation and ruptured of the microcapsules. Moreover, in order to mimic the actual mechanical attack during enzymatic reaction, moderate amount of bovine serum albumin (BSA) were encapsulated in each kind of microcapsules. Table 1 demonstrated that $(Protamine/PSS)_4$ SCMCs first ruptured as the PSS concentration reached 8 wt %. Under identical condition, few ruptured microcapsules were observed for the $(Protamine/O\text{-}alginate)_4$ SCMCs. When the PSS concentration increased to 12 wt %, most of the $(O\text{-}alginate/Protamine)_4$ SCMCs became ruptured, but no deformation could be observed for the organic DMMCs and HDMMCs. As PSS concentration increased to 20 wt %, most of the organic DMMCs were deformed; however, the HDMMCs still preserved regular sphere shape. Thus, the order of the mechanical stability was derived as follows: HDMMCs > Organic DMMCs>-$(Protamine/O\text{-}alginate)_4$ SCMCs>$(Protamine/PSS)_4$ SCMCs. The much higher mechanical stability for HDMMCs should be attributed to the unique structure and hybrid materials. Specifically, (1) the inner membrane was fabricated via electrostatic and covalent interaction; (2) the rigid organic−inorganic hybrid outer membrane were more deformation-resistant;[37,38] (3) additionally, during the removal of silica layers, BSA molecules were released into nanoscale intermembrane space and built up an osmotic pressure.[39] This osmotic pressure could partly offset the overall pressure to the interior of capsules from the outside.

3.2. Validation of Multienzyme System Constructed by HDMMCs. In the subsequent work, we explored the possibility of using HDMMCs to construct the multizenzyme system. Considering the high cost of dehydrogenases in particular formaldehyde dehydrogenases, BSA was chosen as a substitute in some experiments. Figure 6 showed the fluorescence microscope images of the HDMMCs with FITC-labeled BSA encapsulated in microscale lumen (Figure 6a) and nanoscale intermembrane space (Figure 6b). The fluorescence signal revealed the successful encapsulation of BSA at the target positions. BSA loading capacity in the lumen was about 300 μg mg $(HDMMCs)^{-1}$. Then, protamine was adsorbed on the inner membrane to induce the hydrolysis and condensation of silicate, while BSA molecules were entrapped accompanying with the formation of the silica particles.[40,41] Thus, BSA loading capacity in the intermembrane space depended upon a number of factors, such as BSA concentration, silicate concentration, additive concentration (the

relevant data were shown in Figure S4 of the Supporting Information). First, BSA loading capacity increased sharply and gradually leveled off as a function of BSA concentration. As BSA concentration reached 1.0 mg mL^{-1}, 185 μg mg $(HDMMCs)^{-1}$ BSA could be immobilized in intermembrane space. Then, as silicate concentration increased from 10 to 70 mM, BSA loading capacity increased from 61 μg mg $(HDMMCs)^{-1}$ to ca. 180 μg mg $(HDMMCs)^{-1}$. Finally, as shown in Figure S4c in the Supporting Information, BSA loading capacity first increased and then decreased as Ca^{2+} concentration increased from 0.05 to 0.8 mg mL^{-1}. The maximum loading capacity of 280 μg mg $(HDMMCs)^{-1}$ located at 0.1 mg mL^{-1} of Ca^{2+} concentration.

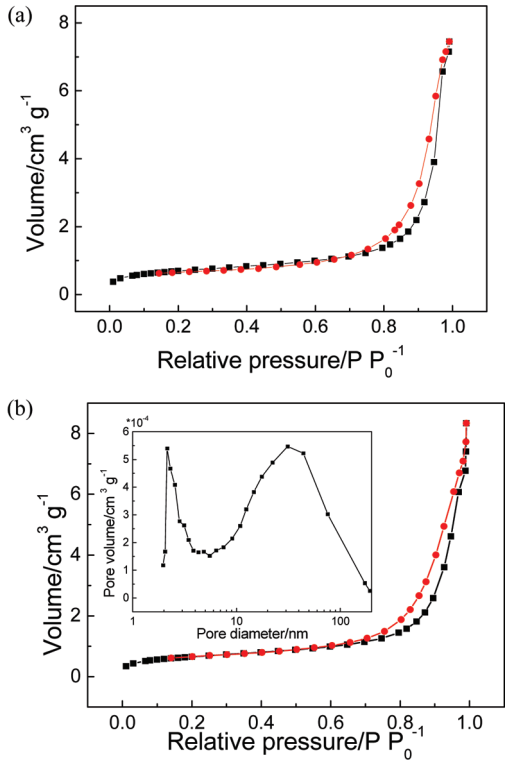

Figure 5. Nitrogen adsorption−desorption isotherms (inset is the pore size distribution curve by the BJH method) of (a) the inner membrane and (b) HDMMCs.

To further elucidate this application potential and advantages of the HDMMCs, we employed cascade reaction comprising two types of enzymes that could convert CO_2 to formaldehyde under mild conditions. Overall, the conversion involved an initial reduction of CO_2 to formic acid by FateDH and the subsequent reduction of formic acid to formaldehyde by FaldDH. NADH acted as a terminal electron donor for each step. The reaction rate calculations were based on the NADH consumption rate at the time of *t*, and the selectivity calculations were based on the fact that 1 mol of formaldehyde consumes 2 mols of NADH. Cascade reactions were carried out at each enzyme concentration about 0.3 mg of protein mL^{-1}, whereas the concentration of NADH varied in the range of 50−200 mM (as shown in Figure S5 of the Supporting Information). For comparison, the same amount of the two enzymes freely in aqueous solution and coencapsulated in the $(Protamine/O\text{-}alginate)_4$ SCMCs also underwent the catalytic activity evaluation.

The NADH consumption and formaldehyde product as a function of time as well as the reaction rate of free and immobilized enzymes in the SCMCs and HDMMCs was shown in Figure 7. The free multienzyme system produced the higher formaldehyde product during the first two hours and exhibited higher reaction rate during the first hour, but the reaction rate quickly decreased to zero because of the existence of reaction equilibrium. The reaction rate of the HDMMCs system was higher than that of SCMCs during all the time. The formaldehyde product in the SCMCs and HDMMCs was significantly higher compared to free enzymes after equilibrium, indicating

Table 1. Mechanical Stability of Four Types of Microcapsules As a Function of PSS Concentration[a]

PSS concentration (%)	HDMMCs	organic DMMCs	$(Protamine/O\text{-}alginate)_4$ SCMCs	$(Protamine/PSS)_4$ SCMCs
4	no change	no change	no change	no change
8	no change	no change	no change	ruptured
12	no change	no change	ruptured	
20	no change	deformed		

[a] No change: more than 90% of the microcapsules preserved the original shape. Deformed: more than 90% of the microcapsules were deformed. Ruptured: more than 90% of the microcapsules were ruptured.

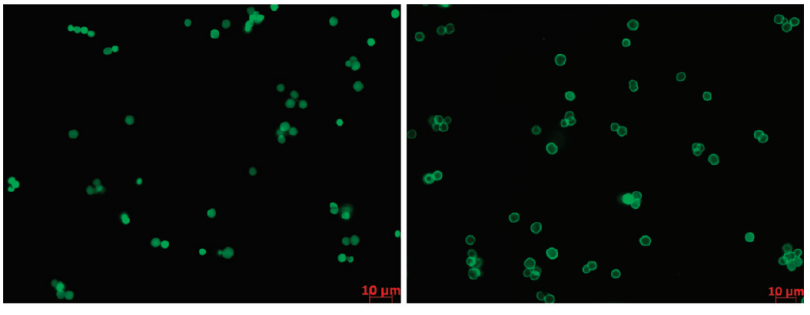

(a) (b)

Figure 6. Fluorescence microscope images of FITC labeled-BSA encapsulated (a) in the microscale lumen and (b) in the intermembrane space of the HDMMCs.

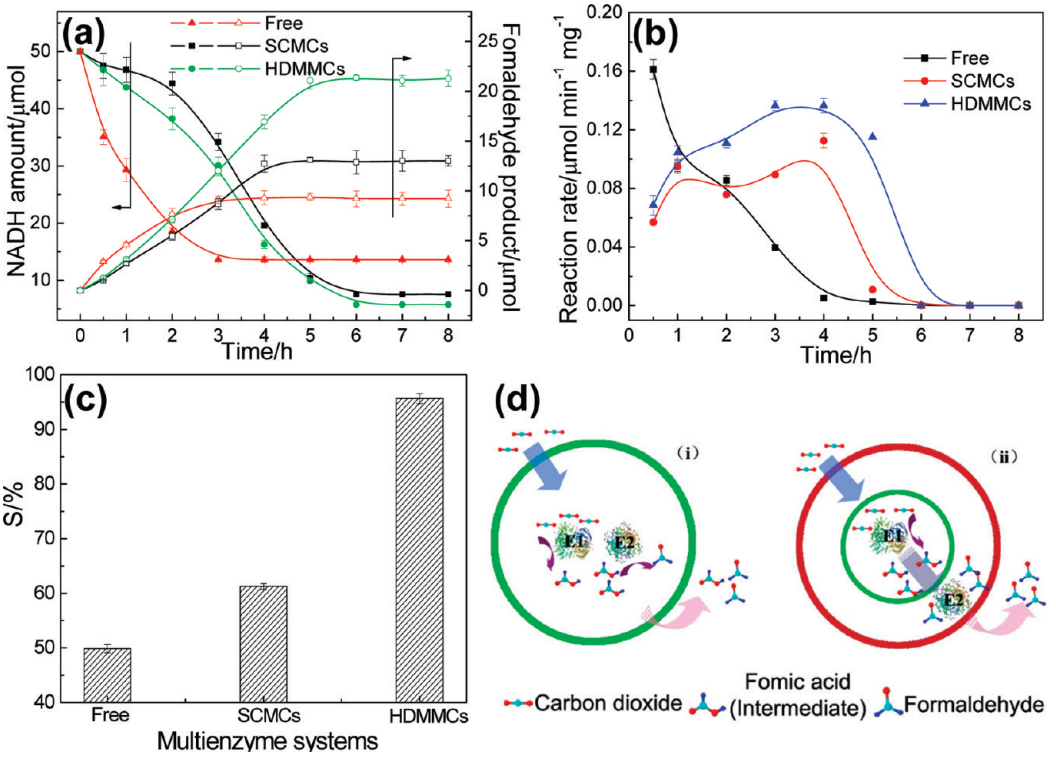

Figure 7. Plot of (a) NADH consumption and formaldehyde product as a function of time; (b) reaction rate of the three types of multienzyme systems as a function of reaction time, and (c) formaldehyde selectivity for different multienzyme systems at equilibrium; (d) proposed mechanism for conversion of CO_2 to formaldehyde in the (i) SCMCs and (ii) HDMMCs.

that the overall equilibrium was shifted more toward the products,[42] which might be as a result of the substantially reduced diffusion distance for the reaction intermediate to travel between the active sites of the enzymes.[43] In addition, the formaldehyde selectivity for enzymes encapsulated in HDMMCs was much higher than that in SCMCs. The tentative explanation for the enhancement of formaldehyde product and selectivity was presented in Figure 7d (ii), CO_2 transferred through the outer membrane/intermembrane space/inner membrane into the lumen to be converted to formic acid. The formic acid had to go through the inner membrane/intermembrane space/outer membrane to escape, which ensured that all of the formic acid molecules won enough time to contact with FaldDH and to convert into formaldehyde. As a result, the formaldehyde product and selectivity was increased sharply.[44] But for the cascade reaction in the SCMCs (Figure 7d (i)), portion of the intermediate would diffuse out of the microcapsule without contacting with FaldDH, and the product and selectivity were thus much lower.

Meanwhile, the formaldehyde product with recycling times of the immobilized enzymes was evaluated as shown in Figure 8. Compared to the dehydrogenases encapsulated in the SCMCs, the activity and recycling stability of dehydrogenases encapsulated in the HDMMCs was significant improved. This was mainly due to (1) the interference between different enzymes was reduced or even eliminated by spatially separated immobilization, which resulted in a higher formaldehyde yield; (2) compared with the organic SCMCs, the HDMMCs with higher mechanical and structural stability can deter the microcapsule breakage after treatments under vigorous centrifugation and continuous stirring.

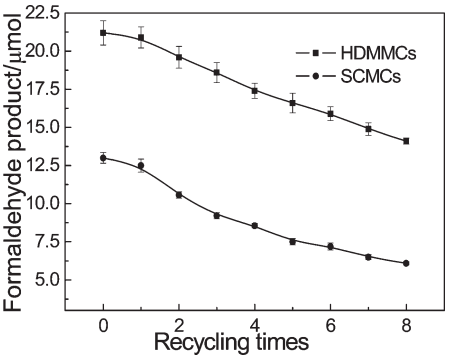

Figure 8. Recycling stability of the enzymes encapsulated in the SCMCs and HDMMCs. The reaction was carried out at following conditions: amount of each enzyme added, 0.3 mg; reaction time, 6 h; temperature, 37 °C.

4. CONCLUSIONS

In summary, mitochondria-inspired double membrane structure has been successfully created through two biocompatible platform technologies, biomimetic mineralization and LbL self-assembly, with the assistance of double hard templates. Two types of enzymes were respectively confined in the lumen and the intermembrane space of the HDMMCs to construct the multienzyme system in a facile and controllable approach. Compared with the single-compartment multienzyme system or free enzyme system, this multicompartment multienzyme system exhibits higher enzyme activity (including highest NADH conversion and formaldehyde product) and stability in the cascade conversion of formaldehyde from CO_2. Hopefully, the double

membrane structure protocol in our study may find some applications in chemical/biological catalysis and separation, drug/gene controlled release, etc.

■ ASSOCIATED CONTENT

Supporting Information. FTIR spectra of alginate and o-alginate, influence of EDTA and NH_4F/HF on the activity of the free multienzyme system, permeability of the inner membrane and the outer membrane, loading capacity of BSA in the intermembrane space of the HDMMCs, product and yield of formaldehyde with respect to variation of NADH for immobilized multienzyme systems and free multienzyme system. This material is available free of charge via the Internet at http://pubs.acs.org.

■ AUTHOR INFORMATION

Corresponding Author
*E-mail: zhyjiang@tju.edu.cn (Prof. Zhongyi Jiang).

■ ACKNOWLEDGMENT

The authors thank the financial support from the National Basic Research Program of China (2009CB724705), the National Science Foundation of China (20976127), the program for Changjiang Scholars and Innovative Research Team in University (PCSIRT), the Program of Introducing Talents of Discipline to Universities (B06006), and the Open Funding Project of the State Key Laboratory of Bioreactor Engineering.

■ REFERENCES

(1) Moehlenbrock, M. J.; Toby, T. K.; Waheed, A.; Minteer, S. D. *J. Am. Chem. Soc.* **2010**, *132*, 6288–6289.
(2) Conrado, R. J.; Varner, J. D.; DeLisa, M. P. *Curr. Opin. Biotechnol.* **2008**, *19*, 492–499.
(3) Yang, M.; Ma, J.; Zhang, C. L.; Yang, Z. Z.; Lu, Y. F. *Angew. Chem., Int. Ed.* **2005**, *44*, 6727–6730.
(4) Huang, C. C.; Huang, W.; Yeh, C. S. *Biomaterials* **2011**, *32*, 556–564.
(5) Lou, X. W.; Yuan, C. L.; Archer, L. A. *Adv. Mater.* **2007**, *19*, 3328–3332.
(6) Lou, X. W.; Yuan, C. L.; Archer, L. A. *Small* **2007**, *3*, 261–265.
(7) Liu, J.; Hartono, S. B.; Jin, Y. G.; Li, Z.; Lu, G. Q.; Qiao, S. Z. *J. Mater. Chem.* **2010**, *20*, 4595–4601.
(8) Wang, X.; Wu, X. L.; Guo, Y. G.; Zhong, Y. T.; Cao, X. Q.; Ma, Y.; Yao, J. N. *Adv. Funct. Mater.* **2010**, *20*, 1680–1686.
(9) Xu, H. L.; Wang, W. Z. *Angew. Chem., Int. Ed.* **2007**, *46*, 1489–1492.
(10) Liu, J.; Xia, H.; Xue, D. F.; Lu, L. *J. Am. Chem. Soc.* **2009**, *131*, 12086–12087.
(11) Zhang, H. G.; Zhu, Q. S.; Zhang, Y.; Wang, Y.; Zhao, L.; Yu, B. *Adv. Funct. Mater.* **2007**, *17*, 2766–2771.
(12) Wu, Z. C.; Zhang, M.; Yu, K.; Zhang, S. D.; Xie, Y. *Chem.—Eur. J.* **2008**, *14*, 5346–5352.
(13) Li, G. L.; Shi, Q.; Yuan, S. J.; Neoh, K. G.; Kang, E. T.; Yang, X. L. *Chem. Mater.* **2010**, *22*, 1309–1317.
(14) Li, G. L.; Lei, C. L.; Wang, C. H.; Neoh, K. G.; Kang, E. T.; Yang, X. L. *Macromolecules* **2008**, *41*, 9487–9490.
(15) Ladet, S.; David, L.; Domard, A. *Nature* **2008**, *452*, 76–79.
(16) Kreft, O.; Prevot, M.; Mohwald, H.; Sukhorukov, G. B. *Angew. Chem., Int. Ed.* **2007**, *46*, 5605–5608.
(17) Luckarift, H. R.; Spain, J. C.; Naik, R. R.; Stone, M. O. *Nat. Biotechnol.* **2004**, *22*, 211–213.
(18) Pouget, E.; Dujardin, E.; Cavalier, A.; Moreac, A.; Valery, C.; Marchi-Artzner, V.; Weiss, T.; Renault, A.; Paternostre, M.; Artzner, F. *Nat. Mater.* **2007**, *6*, 434–439.
(19) Yang, S. H.; Lee, K. B.; Kong, B.; Kim, J. H.; Kim, H. S.; Choi, I. S. *Angew. Chem., Int. Ed.* **2009**, *48*, 9160–9163.
(20) Jiang, Y. J.; Yang, D.; Zhang, L.; Sun, Q. Y.; Sun, X. H.; Li, J.; Jiang, Z. Y. *Adv. Funct. Mater.* **2009**, *19*, 150–156.
(21) Li, J.; Jiang, Z. Y.; Wu, H.; Zhang, L.; Long, L. H.; Jiang, Y. J. *Soft Matter* **2010**, *6*, 542–550.
(22) Wang, B.; Liu, P.; Jiang, W. G.; Pan, H. H.; Xu, X. R.; Tang, R. K. *Angew. Chem., Int. Ed.* **2008**, *47*, 3560–3564.
(23) Zhang, Y.; Wu, H.; Li, J.; Li, L.; Jiang, Y. J.; Jiang, Y.; Jiang, Z. Y. *Chem. Mater.* **2008**, *20*, 1041–1048.
(24) Jiang, Y. J.; Yang, D.; Zhang, L.; Li, L.; Sun, Q. Y.; Zhang, Y. F.; Li, J.; Jiang, Z. Y. *Dalton Trans.* **2008**, 4165–4171.
(25) Li, L.; Jiang, Z. Y.; Wu, H.; Feng, Y. N.; Li, J. *Mater. Sci. Eng., C* **2009**, *29*, 2029–2035.
(26) van Dongen, S. F. M.; Nallani, M.; Cornelissen, J. J. L. M.; Nolte, R. J. M.; van Hest, J. C. M. *Chem.—Eur. J.* **2009**, *15*, 1107–1114.
(27) Willner, O. I.; Weizmann, Y.; Gill, R.; Lioubashevski, O.; Freeman, R.; Willner, I. *Nat. Nanotechnol.* **2009**, *4*, 249–254.
(28) Jiang, Y. J.; Sun, Q. Y.; Zhang, L.; Jiang, Z. Y. *J. Mater. Chem.* **2009**, *19*, 9068–9074.
(29) Bertrand, P.; Jonas1, A.; Laschewsky, A.; Legras, R. *Macromol. Rapid Commun.* **2000**, *21*, 319–348.
(30) De Geest, B. G.; Déjugnat, C.; Prevot, M.; Sukhorukov, G. B.; Demeester, J.; De Smedt, S. C. *Adv. Funct. Mater.* **2007**, *17*, 531–537.
(31) Tong, W. J.; Dong, W. F.; Gao, C. Y.; Mohwald, H. *J. Phys. Chem. B* **2005**, *109*, 13159–13165.
(32) Csiszar, A.; Hoffmann, B.; Merkel, R. *Langmuir* **2009**, *25*, 5753–5761.
(33) Coradin, T.; Livage, J. *Mater. Sci. Eng., C* **2005**, *25*, 201–205.
(34) Allouche, J.; Boissiere, M.; Helary, C.; Livage, J.; Coradin, T. *J. Mater. Chem.* **2006**, *16*, 3120–3125.
(35) Cui, J.; He, W.; Liu, H.; Liao, S.; Yue, Y. *Colloids Surf., B* **2009**, *74*, 274–278.
(36) Kruk, M.; Jaroniec, M. *Chem. Mater.* **2001**, *13*, 3169–3183.
(37) Podsiadlo, P.; Kaushik, A. K.; Arruda, E. M.; Waas, A. M.; Shim, B. S.; Xu, J. D.; Nandivada, H.; Pumplin, B. G.; Lahann, J.; Ramamoorthy, A.; Kotov, N. A. *Science* **2007**, *318*, 80–83.
(38) Walther, A.; Bjurhager, I.; Malho, J. M.; Pere, J.; Ruokolainen, J.; Berglund, L. A.; Ikkala, O. *Nano Lett.* **2010**, *10*, 2742–2748.
(39) Dai, Z. F.; Mohwald, H.; Tiersch, B.; Dahne, L. *Langmuir* **2002**, *18*, 9533–9538.
(40) Ramanathan, M.; Luckarift, H. R.; Sarsenova, A.; Wild, J. R.; Ramanculov, E. K.; Olsen, E. V.; Simonian, A. L. *Colloids Surf., B* **2009**, *73*, 58–64.
(41) Betancor, L.; Luckarift, H. R.; Seo, J. H.; Brand, O.; Spain, J. C. *Biotechnol. Bioeng.* **2008**, *99*, 261–267.
(42) Obert, R.; Dave, B. C. *J. Am. Chem. Soc.* **1999**, *121*, 12192–12193.
(43) Srere, P. A.; Mattiasson, B.; Mosbach, K. *Proc. Natl. Acad. Sci. U. S.A.* **1973**, *70*, 2534–2538.
(44) Yang, G. H.; Tsubaki, N.; Shamoto, J.; Yoneyama, Y.; Zhang, Y. *J. Am. Chem. Soc.* **2010**, *132*, 8129–8136.